Characterization of gallium-doped CdS thin films grown by chemical bath deposition

Hani Khallaf [a], Guangyu Chai [b], Oleg Lupan [a,c], Lee Chow [a,*], S. Park [a], Alfons Schulte [a]

[a] Department of Physics, University of Central Florida, Orlando, FL 32816, USA
[b] Apollo Technologies, Inc., 205 Waymont Court, Suite 111, Lake Mary, FL 32746, USA
[c] Department of Microelectronics and Semiconductor Devices, Technical University of Moldova, 168 Stefan cel Mare Boulevard, MD-2004, Chisinau, Republic of Moldova

ABSTRACT

Ga-doped CdS thin films, with different [Ga]/[Cd] ratios, were grown using chemical bath deposition. The effect of Ga-doping on optical properties and bandgap of CdS films is investigated. Resistivity, carrier density, and mobility of doped films were acquired using Hall effect measurements. Crystal structure as well as crystal quality and phase transition were determined using X-ray diffraction (XRD) and Micro-Raman spectroscopy. Film morphology was studied using scanning electron microscopy, while film chemistry and binding states were studied using X-ray photoelectron spectroscopy (XPS). A minimum bandgap of 2.26 eV was obtained at [Ga]/[Cd] ratio of 1.7×10^{-2}. XRD studies showed Ga^{3+} ions entering the lattice substitutionally at low concentration, and interstitially at high concentration. Phase transition, due to annealing, as well as induced lattice defects, due to doping, were detected by Micro-Raman spectroscopy. The highest carrier density and lowest resistivity were obtained at [Ga]/[Cd] ratio of 3.4×10^{-2}. XPS measurements detect an increase in sulfur deficiency in doped films.

© 2008 Elsevier B.V. All rights reserved.

1. Introduction

In-situ doping with group III elements has been widely used to decrease the dark resistivity of CdS thin films grown by chemical bath deposition (CBD) [1,2]. The need to such doping is attributed to the fact that CBD-CdS thin films are highly stoichiometric [3,4]. Accordingly, the dark resistivity of CdS films grown by CBD is so high that, in some cases, it was reported to be in the order of 10^8–$10^{10} \Omega$ cm [5–7]. In-situ doping using group III elements such as aluminum, indium, boron, and gallium, is the most suitable approach to tackle this problem where the need for post-deposition treatments, such as ion-implantation, is being eliminated.

In a previous work [8], we have shown that CBD is a suitable technique for aluminum in-situ doping of CdS. We have also shown that due to extremely low solubility product of indium sulfide ($K_{sp} = 10^{-73.24}$) compared to that of CdS ($K_{sp} = 10^{-27.94}$) [9], it is highly unlikely, if not impossible, to incorporate indium in CdS, using CBD. In another work [10], we have investigated boron in-situ doping of CdS using CBD, and proved it to be successful. We have found that, regardless of boron concentration used, B^{3+} ions

tend to replace Cd^{2+} ions in the lattice substitutionally. However, Al^{3+} ions tend to enter the lattice substitutionally at low concentration, and interstitially at high concentration. In both cases, a dark resistivity in the order of $10^{-2} \Omega$ cm and a carrier density as high as 10^{19} cm^{-3} were achieved. The effect of Al-doping as well as B-doping on the optical properties and bandgap of CdS films was investigated. In both cases, bandgap of doped films was found to be always less than that of undoped film. X-ray diffraction (XRD) did not detect any Al or B peaks in doped films indicating that incorporation of Al^{3+} or B^{3+} ions does not affect the crystal structure of CdS film. Phase transition, due to annealing, as well as induced lattice defects, due to doping, were detected in both cases by Micro-Raman spectroscopy. An increase in sulfur deficiency due to doping was detected by X-ray photoelectron spectroscopy (XPS). However, scanning electron microscopy (SEM) micrographs showed morphology of films unaffected by Al or B-doping.

In extension to this work, Gallium in-situ doping of CdS using chemical bath deposition is being reported. The same investigation methodology used in Al/B-doping work [8,10] is being implemented here as well. The objective of this work is mainly to provide a comparison between Ga-doping of CdS and Al/B-doping. Therefore, in addition to using the same characterization techniques, the [dopant]/[Cd] ratio used in this work was exactly the same as that used earlier in B-doping [10]. Similarly, transmittance and reflectance measurements of doped films were carried out to

study the effect of Ga-doping on the optical properties and bandgap of CdS films. Resistivity, carrier concentration, and mobility of doped films were acquired using Hall effect measurements. Crystal structure as well as crystal quality and phase transition were determined using XRD and Micro-Raman spectroscopy. Film morphology was studied using SEM, while film chemistry and binding states were studied using XPS.

2. Experimental details

CdS films were prepared using stock solutions of $CdSO_4$ (0.038 M), $(NH_4)_2SO_4$ (0.076 M), NH_3OH (29.4%), and $(NH_2)_2CS$ (0.076 M). Films were grown on 38 mm × 38 mm × 1 mm glass substrates (Schott Borofloat glass, supplied by S.I. Howard Glass Co., Inc.). Gallium doping was carried out by adding the appropriate amount from a 4 mM stock solution of $Ga(NO_3)_3$ to the main solution. The deposition temperature was kept constant at 85 °C. After deposition, all films were annealed at 300 °C in argon ambient for 1 h. Details of the growth process have been previously reported [4]. The cleaning steps of the substrate are reported elsewhere [8].

Alpha-step 500 surface profilometer (Tencor) was used to determine film thickness. Specular transmittance measurements were carried out at room temperature with unpolarized light at normal incidence in the wavelength range from 350 to 1200 nm using Cary 500 (Varian) double beam UV–vis spectrophotometer. Specular reflectance measurements were carried out at an angle of incidence of 7° in the same wavelength range. The optical absorption coefficient α was calculated for each film using the equation [11]:

$$T = (1 - R)^2 \exp(-\alpha t) \tag{1}$$

where T is transmittance, R is reflectance, and t is film thickness.

The absorption coefficient α is related to the incident photon energy $h\nu$ as:

$$\alpha = \frac{K(h\nu - E_g)^{n/2}}{h\nu} \tag{2}$$

where K is a constant, E_g is the optical bandgap, and n is equal to 1 for direct bandgap material such as CdS. The bandgap was determined for each film by plotting $(\alpha h\nu)^2$ versus $h\nu$ and then extrapolating the straight line portion to the energy axis. XRD was carried out using Rigaku D XRD unit (with 40 kV, 30 mA CuKα radiation, λ = 0.15406 nm). The sample was mounted at 2.5° and scanned from 25°–60° in steps of 0.02° with a scan rate of 1.2° min⁻¹. Resistivity, Hall mobility, and carrier density were evaluated by Hall effect measurements at room temperature in a Van der Pauw four-point probe configuration, using indium contacts, in an automated Hall effect system (Ecopia HMS-3000, Bridge Technology, Chandler Heights AZ, USA) with a 0.55 T magnetic induction. Micro-Raman scattering was performed at room temperature with a Horiba Jobin Yvon LabRam IR system at a spatial resolution of 2 μm in a backscattering configuration. A 632.8 nm line of a Helium Neon laser was used for off-resonance excitation with less than 4 mW power at the sample. The spectral resolution was 2 cm⁻¹, and the instrument was calibrated to the same accuracy using a naphthalene standard. XPS was performed on a Physical Electronics PHI 5400 ESCA using monochromatic MgKα radiation at 1253.6 eV. Each of the XPS spectra was acquired from 30 repeated sweeps. XPS spectra were corrected from charging effects by referencing the adventitious C1s peak to 284.6 eV. SEM micrographs were obtained using JEOL 6400F SEM at an acceleration voltage of 10 kV.

3. Results and discussion

Fig. 1 shows optical transmittance and reflectance spectra of all Ga-doped films grown at different [Ga]/[Cd] ratios. The [Ga]/[Cd] ratio in solution was varied from 8.5 × 10⁻³ to 0.1. Adding higher concentration of $Ga(NO_3)_3$ resulted in a homogeneous reaction that quickly dominated the deposition process and affected the quality of doped-CdS films. It should be noted that a ratio of zero was assigned to undoped film (purely CdS). As shown, all films exhibit a high transmittance that exceeds 80% in the visible region of the spectrum and exceeds 90% right before the absorption edge. A red shift in the absorption edge towards lower band gap is noticed in all Ga-doped films. The magnitude of the red shift was found to fluctuate as [Ga]/[Cd] ratio increases. Using transmittance and reflectance data, the absorption coefficient α was calculated and was then used to determine the bandgap, as shown in Fig. 2. Fig. 3 shows the bandgap dependence on [Ga]/[Cd] ratio. The bandgap of doped films decreases to a minimum of 2.26 eV at a ratio of 0.017, then increases and finally saturates at 2.32 eV as the [Ga]/[Cd] ratio exceeds 0.06. Undoped film has a bandgap of 2.41 eV which agrees well with the 2.42 eV bandgap of single crystal CdS [12]. This is very similar to what we have observed earlier for Al-doped CdS films [8]. It has been suggested by Lokhande and Pawar [13] that, in the case of Al-doped CdS films, incorporation of Al^{3+} ions as well as sulfur deficiency in Al-doped films gives rise to donor levels in the bandgap of CdS. As the Al concentration increases which in turn increases sulfur deficiency, the donor levels become degenerate and merge in the conduction band of CdS, causing the conduction band to extend into the bandgap which reduces the band gap. Similar argument can be used to explain the decrease in bandgap of Ga-doped CdS thin films. The later increase in bandgap for [Ga]/[Cd] ratio higher than 0.04 may be attributed to an increase in lattice strain due to decrease in grain size of Ga-doped films, as will be shown below. We have shown, in a previous work [3], the bandgap of CdS films to be sensitive to lattice strain. Considering the fact that the bandgap of GaS is 3.05 eV and that of Ga_2S_3 is 3.42 eV [14], this rules out any formation of ternary compounds, such as $Cd_xGa_{1-x}S$.

XRD patterns of Ga-doped films and undoped CdS film are shown in Fig. 4. Only one peak is detected which is either the (1 1 1) peak of cubic CdS or the (0 0 2) peak of hexagonal CdS. Cubic CdS is a metastable phase while hexagonal CdS is the stable phase
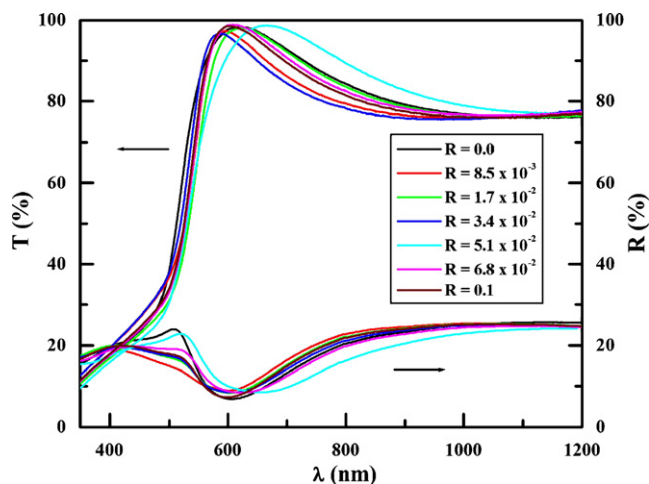

Fig. 1. Specular transmittance and reflectance spectra of Ga-doped CdS films grown at different [Ga]/[Cd] ratios (R denotes [Ga]/[Cd] ratio & R = 0.0 refers to undoped film).
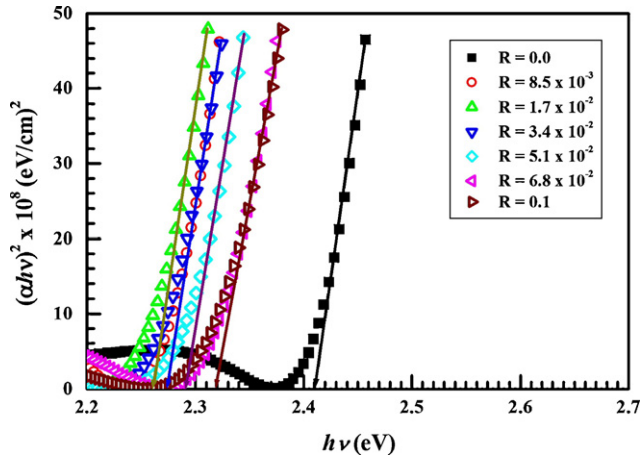
Fig. 2. Optical bandgap calculations of Ga-doped CdS films grown at different [Ga]/[Cd] ratios (R denotes [Ga]/[Cd] ratio & R = 0.0 refers to undoped film).
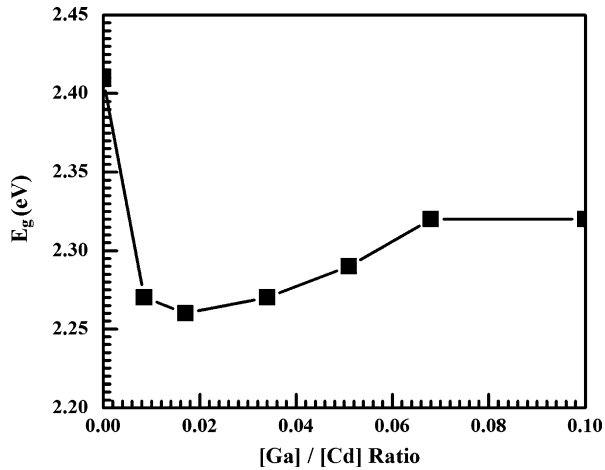

Fig. 3. Optical bandgap of Ga-doped CdS films as a function of [Ga]/[Cd] ratio.
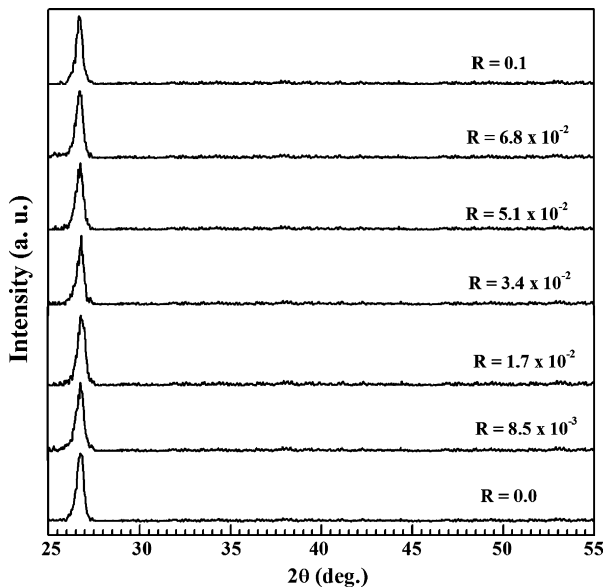

Fig. 4. XRD pattern of Ga-doped CdS films grown at different [Ga]/[Cd] ratios (R denotes [Ga]/[Cd] ratio & R = 0.0 refers to undoped film).
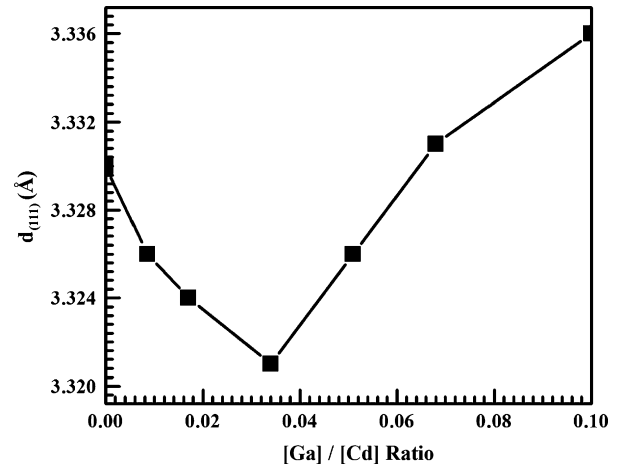

Fig. 5. Average (1 1 1) interplanar distance $d_{(1 1 1)}$ as a function of [Ga]/[Cd] ratio.

at room temperature. Thermal annealing typically causes a phase transition from cubic phase to hexagonal phase. The critical point for such phase transition is believed to be 300 °C [15], above which hexagonal phase predominates over cubic phase. Since no other peaks are detected, it is difficult to determine if the peak shown in Fig. 4 is the (1 1 1) peak of the cubic phase or the (0 0 2) peak of the hexagonal phase which coincides with the (1 1 1) peak. In order to avoid confusion, we will refer to the peak detected as the (1 1 1) peak of cubic CdS. As shown in Fig. 4, no peaks of Ga, GaS, or Ga_2S_3 were detected, which indicates that incorporation of Ga^{3+} ions does not affect the crystal structure of CdS film. This also confirms our conclusion from bandgap calculations of Ga-doped films. The average (1 1 1) interplanar distance $d_{(1 1 1)}$ was calculated using the formula $\lambda = 2d \sin\theta$, where λ is the X-ray wavelength (1.5406 Å), and θ is the Bragg angle. As shown in Fig. 5, as the [Ga]/[Cd] ratio increases, the spacing of the (1 1 1) lattice planes decreases below that of undoped film until it reaches a minimum at a ratio of 0.034 and then it starts to increase as [Ga]/[Cd] ratio increases, and once that ratio exceeds 0.06, the $d_{(1 1 1)}$ value goes beyond that of undoped CdS film. Now, since the ionic radius of Ga^{3+} (0.62 Å) is smaller than that of Cd^{2+} (0.97 Å) [16], this suggests that at low [Ga]/[Cd] ratio, Ga^{3+} ions replace Cd^{2+} ions in the lattice substitutionally which in turn results in smaller $d_{(1 1 1)}$ value than that of undoped CdS film. As this ratio increases beyond 0.034, Ga^{3+} ions start to enter the lattice both substitutionally and interstitially which caused the $d_{(1 1 1)}$ values to increase again. As [Ga]/[Cd] ratio exceeds 0.06, most Ga^{3+} ions incorporated in the lattice are in interstitial sites which caused $d_{(1 1 1)}$ values to exceed that of undoped film. This will have an impact on the electrical properties of Ga-doped films as Hall measurements will show below. The grain size shown in Fig. 6 was calculated using the formula $D = 0.9 \lambda / \beta \cos\theta$, where β is the full width at half maximum (FWHM) in radians. As shown, the grain size increases with the [Ga]/[Cd] ratio, and then as this ratio exceeds 0.034, the grain size decreases as that ratio increases. This decrease in grain size may have caused lattice strain that resulted in the increase observed in the band gap of doped films grown at [Ga]/[Cd] ratio higher than 0.04, as we mentioned earlier.

Fig. 7 shows the carrier concentration (C.C.) as a function of [Ga]/[Cd] ratio. The undoped film has a C.C. of about 4×10^{16} cm^{-3}. The C.C. increases with [Ga]/[Cd] ratio until it reaches a maximum (~2.96×10^{19} cm^{-3}) at a ratio of 0.034, and then decreases as the ratio exceeds 0.04. The film resistivity as a function of [Ga]/[Cd] ratio is shown in Fig. 8. The dark resistivity drops from $1.03 \times 10^2 \ \Omega$ cm (undoped film) to a minimum of $1.2 \times 10^{-2} \ \Omega$ cm

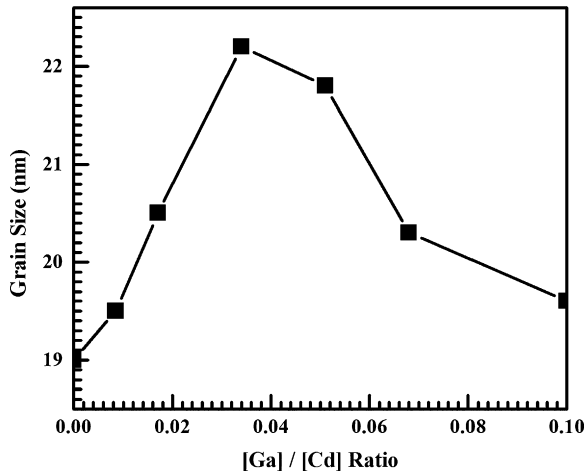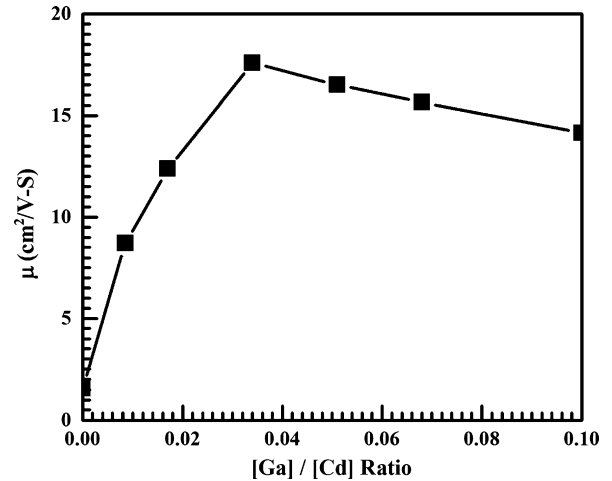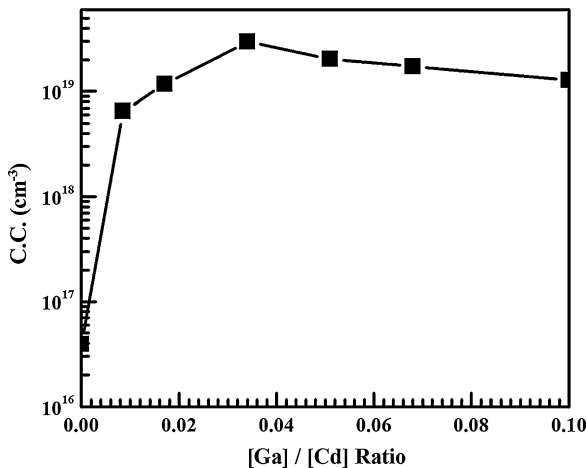**Fig. 6.** Grain size dependence on [Ga]/[Cd] ratio.

Fig. 7. Carrier concentration dependence on [Ga]/[Cd] ratio.

cm at a ratio of 0.034, after which it starts to increase as [Ga]/[Cd] ratio increases. This agrees with the $d_{(1\ 1\ 1)}$ values variation with [Ga]/[Cd] ratio. As we pointed out earlier, at low [Ga]/[Cd] ratios, Ga^{3+} ions replace the Cd^{2+} ions in the lattice substitutionally, which increases the C.C. of the doped films and decreases the resistivity.

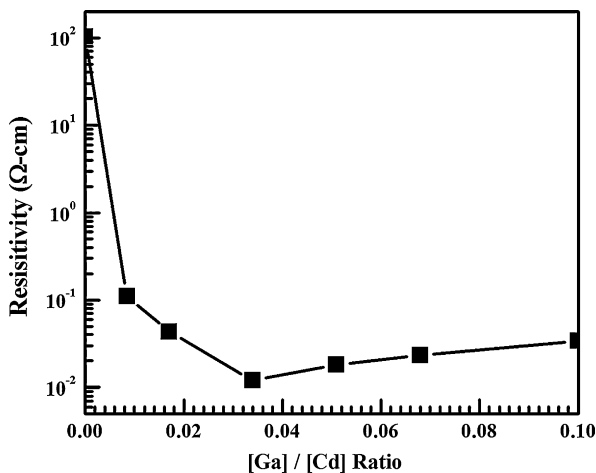**Fig. 8.** Dark resistivity as a function of [Ga]/[Cd] ratio.

Fig. 9. Variation of Hall mobility with [Ga]/[Cd] ratio.

However, at higher ratios, Ga^{3+} ions start to enter the lattice both substitutionally and interstitially. Interstitial Ga^{3+} ions will act as recombination centers decreasing the C.C. and increasing the resistivity. Such behaviour of C.C. as well as dark resistivity has been also reported by Lokhande and Pawar [13] and by Akintunde [17], for Al-doped CdS films. The Hall mobility (μ) values shown in Fig. 9 are consistent with what we reported earlier for Al-doped and B-doped CdS films [8,10]. Variation of μ with respect to [Ga]/[Cd] ratio agrees with the way grain size changes with respect to [Ga]/[Cd] ratio (Fig. 6).

Fig. 10 shows Micro-Raman spectra for all Ga-doped CdS films. All films show the same CdS characteristic peak at about 303 cm^{-1}. Another CdS characteristic peak; 2LO (longitudinal optical) is barely noticeable at about 600 cm^{-1}. As shown, the peak at 303 cm^{-1} is asymmetric; suggesting a superposition of more than one mode. Fig. 11 shows the deconvolution of the 303 cm^{-1} peak of film grown at [Ga]/[Cd] ratio of 6.8×10^{-2}, using Gaussian fit from which peak position and FWHM have been obtained. Similar to what we have observed in Al-doped and B-doped films [8,10], this peak consists of a superposition of three different peaks; the cubic 1LO [18] or hexagonal $A_1(LO)/E_1(LO)$ peak [19] at 303.2 cm^{-1} with
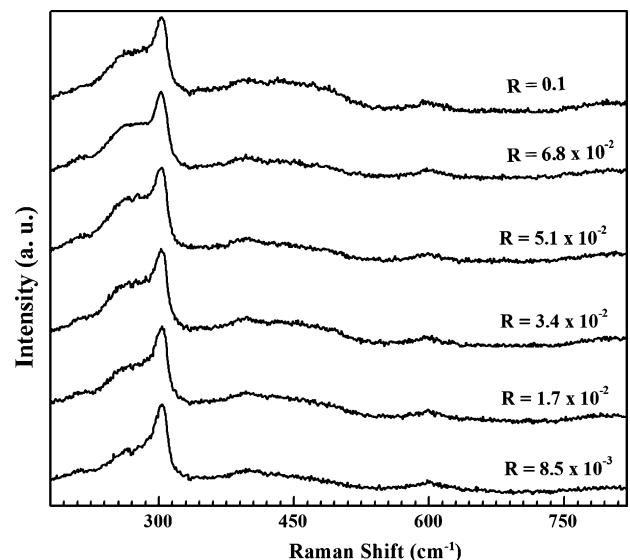

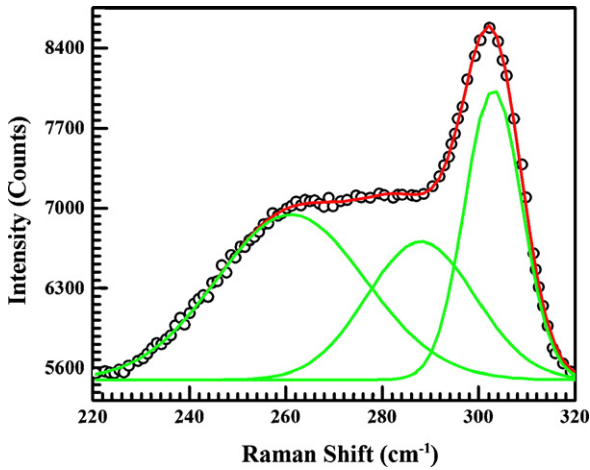**Fig. 10.** Raman spectra of Ga-doped films grown at different [Ga]/[Cd] ratio (R denotes [Ga]/[Cd] ratio).

Fig. 11. Deconvolution of the 303 cm^{-1} Raman peak of CdS film grown at [Ga]/[Cd] ratio of 6.8×10^{-2} into three peaks using Gaussian fit.
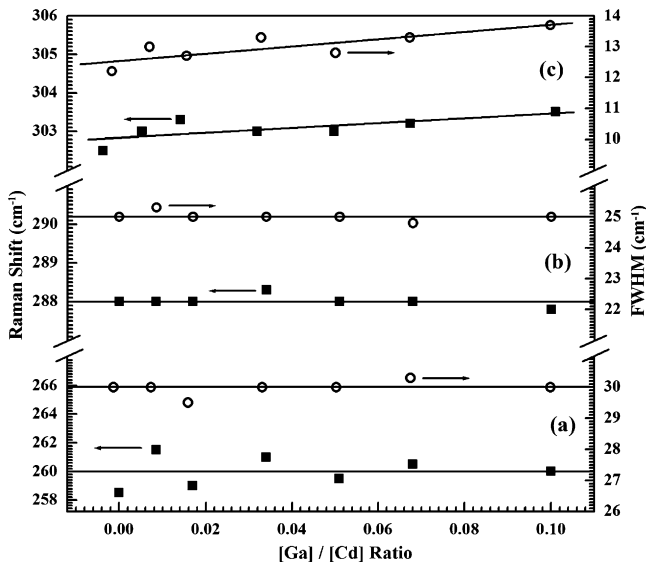

Fig. 12. Peak position and FWHM as a function of [Ga]/[Cd] ratio. (a) E$_2$ peak of hexagonal CdS. (b) Shifted TO peak of cubic CdS. (c) Cubic 1LO or hexagonal A$_1$(LO)/E$_1$ (LO) peak.

a FWHM of 13.3 cm^{-1}, the shifted TO (Transverse Optical) peak of cubic CdS at 288 cm^{-1} with a FWHM of 24.8 cm^{-1}, and the E$_2$ peak of hexagonal CdS at 260.5 cm^{-1} with a FWHM of 30.3 cm^{-1}. This Raman shift in the TO peak (originally at 246 cm^{-1} [18]) is due to a phase transition in CdS film, from cubic to hexagonal, because of the annealing at 300 °C [8]. So, unlike XRD, Micro-Raman detects a phase transition in CdS due to annealing. We have shown earlier that this phase transition is attributed to annealing rather than doping [8].

Similar deconvolution of the 303 cm^{-1} peak was carried out for all Ga-doped films. Fig. 12 shows position and FWHM of the E$_2$, TO, and cubic 1LO or hexagonal A$_1$(LO)/E$_1$(LO) peaks calculated from the Gaussian fit, as a function of [Ga]/[Cd] ratio. Apparently, the position and FWHM of both the E$_2$ and TO peaks are on the average constant regardless of the [Ga]/[Cd] ratio used. The average position of the E$_2$ peak was found to be 260 cm^{-1} (Fig. 12 a) which is slightly higher than what we observed for Al-doped (258.3 cm^{-1}) and B-doped (258 cm^{-1}) films [8,10], but still agrees with the 256 cm^{-1} [20] and the 257 cm^{-1} [21] value of E$_2$ mode that has been reported earlier. The average position of the TO peak (Fig. 12 b) is 288 cm^{-1} which is the same Raman shift observed for both Al-doped and B-doped CdS thin films [8,10]. However, as shown in Fig. 12 (c), the position and FWHM of the cubic 1LO or hexagonal A$_1$(LO)/E$_1$(LO) peak are sensitive to [Ga]/[Cd] ratio. As the ratio increases, peak position and FWHM increase. The increase in FWHM is, however, more significant which implies an increase in induced lattice defects as [Ga]/[Cd] ratio increases. As shown, FWHM increases from 12.2 cm^{-1} for undoped CdS to 13.7 cm^{-1} for film grown at [Ga]/[Cd] ratio of 0.1. It is worth noting that FWHM of the 1LO phonon of single crystal CdS was reported to be in the range of 9–10 cm^{-1} [22].

Fig. 13 shows XPS multiplex spectra for undoped film, and Ga-doped film grown at [Ga]/[Cd] ratio of 5.1×10^{-2}. In both cases, binding energy of the S 2p peak (Fig. 13 a) is 161.7 eV which is in the range characteristic of sulfides. No peak shift was detected due to B-doping. Also, no sulfur oxides (166–171 eV) or elemental sulfur (164 eV) [23] are observed. The presence of two peaks arises from a spin orbit splitting of 1.18 eV between the S 2p$_{1/2}$ and the S 2p$_{3/2}$ states. Similarly, the binding energy of the Cd 3d$_{5/2}$ peak at 405.0 eV (Fig. 13 b) was found to be the same for both films. The binding energy of the Cd 3d$_{3/2}$ peak was 411.7 eV, which agrees with the well-known energy splitting of 6.74 eV between Cd 3d$_{5/2}$ and Cd 3d$_{3/2}$ states [23]. Both values of binding energy for S 2p and Cd 3d peaks observed in both films agree well with previously
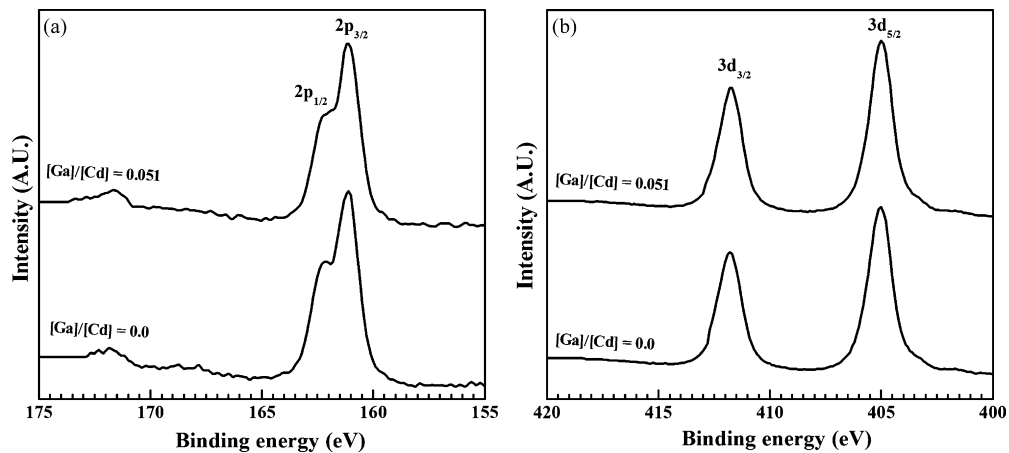

Fig. 13. XPS multiplex spectra of undoped CdS film, and Ga-doped film grown at [Ga]/[Cd] ratio of 5.1×10^{-2}. (a) S 2p peak. (b) Cd 3d peak.
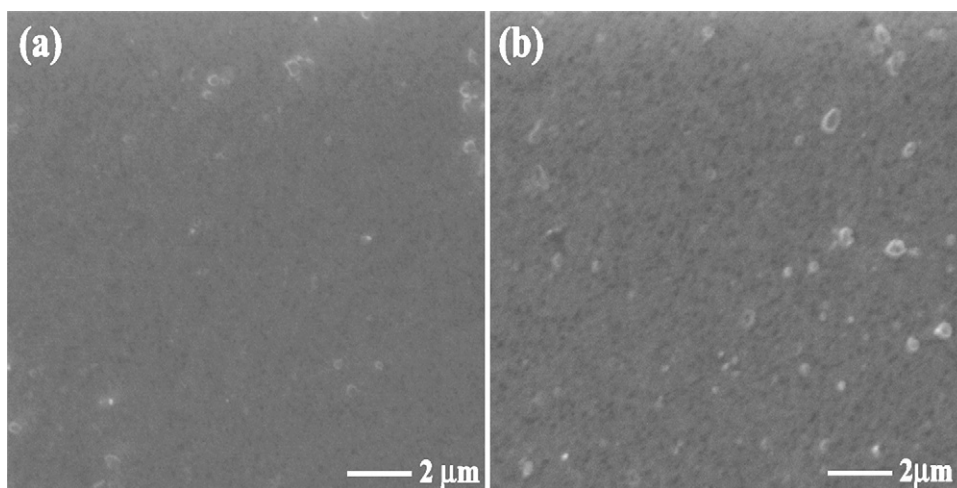
Fig. 14. SEM micrographs of (a) CdS undoped film, and (b) Ga-doped film grown at [Ga]/[Cd] ratio of 1.7×10^{-2}.

reported data on single crystal and thin film CdS [24,25]. It is worth noting that the ratio of S $2p_{3/2}$ signal intensity to that of Cd $3d_{5/2}$ signal was 0.154 for undoped film and became 0.151 for Ga-doped film. Such drop in ratio is similar to what we observed for Al-doped films [8], where it decreased in the order: 0.154, 0.149, and 0.146 as [Al]/[Cd] ratio increased in the order 0.000 (undoped film), 0.036, and 0.180 respectively. This shows that, similar to Al-doping, Ga-doping increases sulfur deficiency in doped films.

SEM images show that Ga-doping did not have a significant effect on the morphology of CdS film. As shown in Fig. 14, both undoped and Ga-doped films are smooth, continuous, and uniform with some coverage by scattered crystallite overgrowth that appear to have slightly higher density for Ga-doped film. These are most probably aggregates due to colloidal particles formed in solution and then adsorbed on the film.

4. Conclusion

Gallium in-situ doping of CdS using CBD proves to be successful. A resistivity as low as $1.2 \times 10^{-2} \, \Omega$ cm and a carrier concentration as high as $2.96 \times 10^{19} \, \text{cm}^{-3}$ have been achieved. The bandgap of doped films was found to decrease at first with Ga concentration and then saturates at 2.32 eV. The minimum bandgap observed was 2.26 eV at [Ga]/[Cd] ratios of 0.017. XRD measurements did not detect any new peaks due to Ga-doping indicating that incorporation of Ga^{3+} ions does not change the crystal structure of the CdS film. It also showed that at low [Ga]/[Cd] ratio, Ga^{3+} ions may replace Cd^{2+} ions in the lattice substitutionally, and as this ratio increases beyond 0.034, Ga^{3+} ions start to enter the lattice both substitutionally and interstitially, until that ratio exceeds 0.06 where most, if not all, Ga^{3+} ions incorporated in the lattice occupy interstitial sites. This explains the drop in carrier concentration and rise in resistivity once the [Ga]/[Cd] ratio exceeds 0.034. Micro-Raman measurements show phase transition in all films, due to annealing, where modes of cubic and hexagonal phases were detected. An increase in the FWHM of cubic 1LO or hexagonal $A_1(LO)/E_1(LO)$ peak with [Ga]/[Cd] ratio was observed, which implies an increase in induced lattice defects as [Ga]/[Cd] ratio increases. XPS spectra showed that, however Ga-doping did not cause any shift in the position of the S 2p and Cd 3d peaks, it

increased sulfur deficiency in doped films. SEM images showed that Ga-doping did not affect the morphology of the CdS film.

References

[1] T. Chu, S. Chu, N. Schultz, C. Wang, C. Wu, J. Electrochem. Soc. 139 (1992) 2443.
[2] J. Lee, Thin Solid Films 451–452 (2004) 170.
[3] H. Khallaf, I. Oladeji, L. Chow, Thin Solid Films 516 (2008) 5967.
[4] H. Khallaf, I. Oladeji, G. Chai, L. Chow, Thin Solid Films 516 (2008) 7306.
[5] C. Guillén, M. Martínez, J. Herrero, Thin Solid Films 335 (1998) 37.
[6] M. Nair, P. Nair, J. Campos, Thin Solid Films 161 (1988) 21.
[7] H. Metin, R. Esen, Semicond. Sci. Technol. 18 (2003) 647.
[8] H. Khallaf, G. Chai, O. Lupan, L. Chow, S. Park, A. Schulte, J. Phys. D: Appl. Phys. 41 (2008) 185304.
[9] L. Sillén, A. Martell, Stability Constants of Metal-Ion Complexes, Burlington House, London, 1964.
[10] H. Khallaf, G. Chai, O. Lupan, L. Chow, S. Park, A. Schulte, Phys. Status Solidi A, doi:10.1002/pssa.2008.24290.
[11] J. Pankove, Optical Processes in Semiconductors, Dover Publications, New York, 1971
[12] S. Sze, Physics of Semiconductor Devices, John Wiley & Sons, New York, 1981.
[13] C. Lokhande, S. Pawar, Solid State Commun. 44 (1982) 1137.
[14] M. Lazell, P. O'Brien, D. Otway, J. Park, J. Chem. Soc., Dalton Trans. (2000) 4479.
[15] O. Zelaya-Angel, J. Alvarado-Gil, R. Lozada-Morales, H. Vargas, A. Ferreira da Silva, Appl. Phys. Lett. 64 (1994) 291.
[16] J. Huheey, Inorganic Chemistry, 3rd edn, Harper & Row, New York, 1983.
[17] J. Akintunde, J. Mater. Sci.: Mater. Electron. 11 (2000) 503.
[18] D. Zahn, C.H. Maierhofer, A. Winter, M. Reckzügel, R. Srama, A. Thomas, K. Horn, W. Richter, J. Vac. Sci. Technol. B 9 (1991) 2206.
[19] B. Tell, T. Damen, S. Porto, Phys. Rev. 144 (1966) 771.
[20] C. Arguello, D. Rousseau, S. Porto, Phys. Rev. 181 (1969) 1351.
[21] M. Nusimovici, J. Birman, Phys. Rev. 156 (1967) 925.
[22] M. Froment, M. Bernard, R. Cortes, B. Mokili, D. Lincot, J. Electrochem. Soc. 142 (1995) 2642.
[23] J. Moulder, W. Stickle, P. Sobol, K. Bomben, in: J. Chastain (Ed.), Handbook of X-ray Photoelectron Spectroscopy, Perkin-Elmer Corporation, Minnesota, 1992.
[24] P. Rieke, S. Bentjen, Chem. Mater. 5 (1993) 43.
[25] M. Marychurch, G. Morris, Surf. Sci. 154 (1985) (1985) L251.